n-Type Charge Transport and Mobility of Fluorinated Perylene Bisimide Semiconductors

Eugenio Di Donato,[†,‡] Rocco P. Fornari,[†,‡] Simone Di Motta,[†,‡] Yan Li,[§] Zhaohui Wang,[§] and Fabrizia Negri*[,†,‡]

Dipartimento di Chimica 'G. Ciamician', Università di Bologna, Via F. Selmi, 2, 40126 Bologna, Italy, INSTM, UdR Bologna, Italy, and Beijing National Laboratory for Molecular Sciences, Key Laboratory of Organic Solids, Institute of Chemistry, Chinese Academy of Sciences, Beijing 100080, People's Republic of China

Received: February 03, 2010; Revised Manuscript Received: March 17, 2010

The intramolecular and intermolecular charge transport parameters are evaluated quantum chemically for three fluorinated derivatives of perylene bisimide (PBI) semiconductors, two of which feature a twisted PBI core. Charge transfer rates are computed within the Marcus−Levich−Jortner formalism including a single effective mode treated quantum mechanically and are injected in a kinetic Monte Carlo scheme to propagate the charge carrier in the crystal and to estimate charge mobilities at room temperature. The relative order of computed mobilities agrees with the observed trend, and the largest mobility is computed for the planar PBI derivative. It is suggested that thermally induced disorder effects should contribute considerably to the observed large mobility of the planar PBI derivative, while a retardation effect induced by the presence of alternating slow and fast jumps along π-stacked PBI columns is responsible for the lower mobilities of the two twisted derivatives. The computed parameters reveal the subtle interplay between intramolecular and intermolecular contributions to the charge carrier propagation in these organic semiconductors and may guide the design of more efficient architectures.

1. Introduction

Organic electronics has been a field of intense research interest for the last couple of decades. Because of their high band gap and low electronic affinity, most of the "classical" organic semiconductors (pentacene, anthracene, phthalocyanines, and most of the conjugated polymers) are p-type or hole-transporting. Among n-type organic semiconductors, derivatives of perylene-3,4:9,10-tetracarboxylic acid bisimides (PBIs) are of increasing interest, due to their exceptional optical and electronic properties, and they have been used in a variety of device architectures in different areas of organic electronics.[1−3] PBI derivatives have also been used as building blocks toward the construction of graphene nanoribbons,[4−7] and side substitution at the bay and imide positions has been used to improve their n-type character and to tune packing and functional properties.[8−13] In this regard, we note that packing and intermolecular arrangement of PBI derivatives have been extensively investigated[14−16] both experimentally and theoretically.

A successful strategy to enhance the n-type character of an organic semiconductor is to functionalize the conjugated core with fluorine atoms[8−10,17] or fluoroalkylated side chains.[18] A thorough analysis of the charge transport properties of halogenated PBIs has been presented by Bao and Wurthner.[9] Among several investigated PBI derivatives, the compound labeled **1a** in ref 9 and in Figure 1 was shown to display a very promising charge mobility. Recently, a convenient synthesis of core-perfluoroalkylated PBIs has been proposed[18] along with the determination of a molecular packing arrangement in single crystals and preliminary charge mobility (n-type) measurements[18] for the PBI derivatives labeled **2b** and **2c** in ref 18 and Figure 1. The observed mobilities are 0.003 $cm^2/(V\ s)$ for compound **2b**,[18] 0.052 $cm^2/(V\ s)$ for compound **2c**,[18] and 0.67−0.72 $cm^2/(V\ s)$ for compound **1a**.[9]

The large variation of measured mobilities points to a combined effect of intramolecular and intermolecular effects. The purpose of this work is to investigate the role of intra- and intermolecular parameters on the charge transport properties of the two recently synthesized core-perfluoroalkylated PBIs featuring different substituents and a twisted PBI core (compounds **2b**,**c** in Figure 1) and whose charge mobilities have been shown to be different.[18] At the same time, a comparison is made with one of the better performing PBI derivatives featuring highly fluorinated imide substituents but only hydrogens in the bay region and a planar PBI core (compound **1a** in Figure 1). To this end, an integrated approach involving quantum-chemical evaluation of inter- and intramolecular parameters combined with kinetic Monte Carlo (KMC) simulations for the propagation of the charge carriers in the crystals was employed to estimate charge mobilities and to provide structure−property relationships.

2. Methods

2.1. Modeling Intra- and Intermolecular Parameters and Charge Transfer Rate Constants. Equilibrium structures of neutral and charged species were obtained from quantum-chemical calculations carried out at B3LYP/6-31G* and B3LYP/3-21G levels of theory. The nature of the critical points determined by quantum-chemical structure optimizations was assessed by evaluating vibrational frequencies at the optimized geometries. Vibrational frequencies were also employed to estimate the vibrational contributions to the intramolecular reorganization energies[19,20] (see below).

Vertical electron affinities (VEA) of PBI derivatives were directly estimated as energy differences between neutral and

* To whom correspondence should be addressed. E-mail: fabrizia.negri@unibo.it.
† Università di Bologna.
‡ INSTM.
§ Chinese Academy of Sciences.

10.1021/jp101040r
Published on Web 04/07/2010

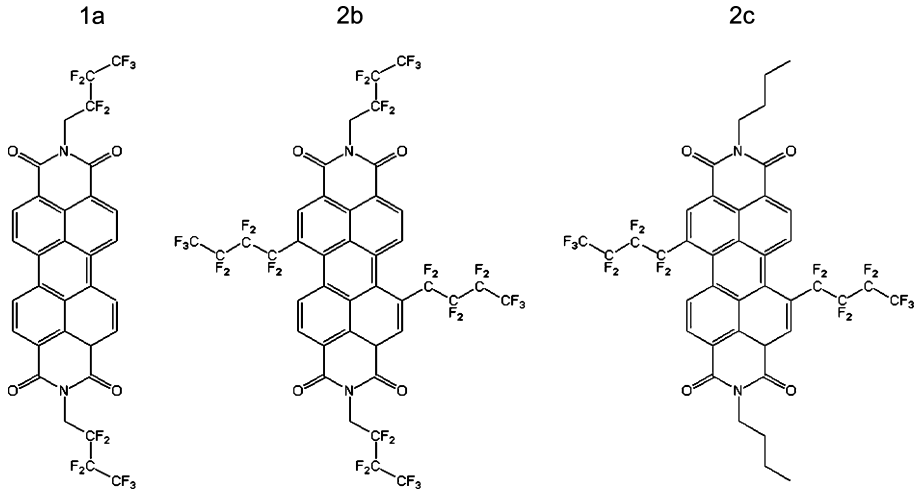

Figure 1. Structural formula of the three PBI derivatives considered in this work.

charged species both computed at the geometries optimized for the neutral (VEAn) or the charged (VEAc) species (see also Figure S1 of the Supporting Information). The intramolecular contribution to the reorganization energy λ_i was computed with the B3LYP functional, either with the adiabatic potential (AP) approach[19,21] (see Figure S1 and Table S1 in the Supporting Information) or via calculations of Huang−Rhys (HR) parameters S_m.[19,21] The charge transfer integrals V_{ij}' were computed at the B3LYP/3-21G level of theory following the direct approach described in refs 22−24. The computed transfer integrals V_{ij}' were transformed in an ortogonalized basis (V_{ij}) as described in previous studies.[25] All of the quantum-chemical calculations were carried out with the Gaussian03 suite of programs.[26]

Bulk charge transport was assumed to be governed by the hopping mechanism.[19,20] The validity of the nonadiabatic hopping model depends on the relative magnitude of the charge transfer integral V_{ij} and the reorganization energy parameter λ, with V_{ij} required to be considerably smaller than λ.[20,27] As it will be shown, we are within, although close to this limit, for the molecules investigated. We are confident, however, that for the purpose of this work, which is to provide structure−property relationships and not absolute values of charge mobilities, the model retains its validity. Furthermore, the hopping contribution should become dominant for the molecules investigated here, in the high temperature regime, which is the one considered in this work. In this scheme, the relevant charge transfer event is localized on a molecular pair (dimer) formed by two neighboring molecules. The organic semiconductor material was taken in its crystalline form, and the possible dimers were identified by evaluating the distances between the centers of mass of the molecules surrounding a central reference molecule in the crystal. A view of the crystals of **1a**, **2b**, and **2c** PBI derivatives is shown in Figure S2 of the Supporting Information, from which it can be seen that the PBI molecules assemble into π-stacked PBI columns in all of the systems investigated.

The transfer rate constants k_{eT} associated with each hopping event were computed according to the Marcus−Levich−Jortner (MLJ) formulation:[28,29]

$$k_{eT} = \frac{2\pi}{\hbar} V_{ij}^{\,2} \frac{1}{\sqrt{4\pi\lambda_{class}k_B T}} \sum_{v=0}^{\infty} \left[\exp(-S_{eff}) \frac{S_{eff}^{v}}{v!} \times \exp\left(- \frac{(\Delta G^{o} + \lambda_{class} + v\hbar\omega_{eff})^2}{4\lambda_{class}k_B T} \right) \right] \quad (1)$$

In the expression above, beside the charge transfer integrals V_{ij}, λ_{class} is the classical contribution (generally the outer sphere contribution) to the reorganization energy and ΔG^{o} is zero for the self-exchange processes considered in this work ($M^{o} + M^{c} \leftrightarrow M^{c} + M^{o}$, where M^{o} is the organic species in the neutral state and M^{c} is the organic species in its charged state). Equation 1 includes the quantum description of the nonclassical degrees of freedom represented by a single effective mode of frequency, ω_{eff}, and associated HR factor, S_{eff}.

2.2. Propagation of Charge Carriers and Evaluation of Charge Mobilities. Charge mobilities were computed assuming a Brownian motion of the charge carrier[30] in the absence of applied electric fields, that is, in the limit of zero field and zero concentration. The calculation of the macroscopic parameter was performed by considering the three-dimensional crystal structures of **1a**, **2b**, and **2c** and by computing the diffusion coefficient D with a set of KMC simulations.[31−33] The KMC technique has been used recently to compute charge mobilities in supermolecular assemblies.[14,34−37] In each KMC simulation, a single charge carrier was let move on the crystal via hopping events occurring between near neighbor molecules, forming a dimer. The probability P_n associated with the hopping event that moves the charge carrier to the n neighbor of a given molecule was determined by the MLJ charge transfer rate constant k_n as $P_n = (k_n/\sum_j k_j)$, where j runs over possible paths for a charge localized on a given molecular unit in the crystal. The time associated with the electron transfer to the n-th neighbor is $1/k_n$, and the distance is the distance between the centers of mass of the two molecules forming the dimer. The trajectory is propagated by selecting randomly one molecule in the crystal as the starting point. A list of possible neighbors is available, and the trajectory is advanced by choosing a random number r uniformly distributed between 0 and 1 and by selecting the j-th neighbor such that[31−33,38] $\sum_n^{j-1} P_n < r \leq \sum_n^{j} P_n$. The position of the charge carrier was saved and accumulated for groups of 2000 trajectories. An approximately linear dependence[31−33] of the mean square displacement (MSD) $\langle [r(t) - r(0)]^2 \rangle$ as a function of time t was obtained by averaging over the subsets of 2000 KMC trajectories (see a representative example in Figure S3 in the Supporting Information). The diffusion coefficient D was readily obtained from the fitted linear dependence of the MSD employing the Einstein equation: $D = \lim_{t\to\infty}(\mathrm{MSD}/6t)$. Charge mobility was obtained from D with the Einstein−Smoluchowski equation:

$$\mu = \frac{eD}{k_B T} \quad (2)$$

Fifteen subgroups of 2000 trajectories each were produced, and the final charge mobilities were obtained by averaging over those computed for each subgroup. Each KMC trajectory consisted of 10^6-10^8 moves, and the temperature T was set to 300 K.

3. Results and Discussion

3.1. Intramolecular Charge Transport Parameters. From the equilibrium structures of neutral and charged species, we estimated both electron affinities and intramolecular reorganization energies (see Figure S1 in the Supporting Information) of the three species **1a**, **2b**, and **2c**. The inclusion of fluoroalkyl substituents in the bay region, for compounds **2b** and **2c**, leads to a marked twist of the perylene core, as well-known for other bay-substituted PBIs.[39] Fluoroalkyl substitution at both the imide and the bay positions lowers the energy of the lowest unoccupied molecular orbital (LUMO) level and increases the electronic affinity of the PBI derivative, thereby strengthening the n-type character of the semiconductor. This effect can be appreciated by considering the energies of the LUMO levels reported in Table S2 in the Supporting Information and the correspondigly computed vertical and adiabatic EAs in Table S3 in the Supporting Information. The inclusion of fluoroalkyl chains (from **1a** to **2b**) in the bay region lowers the LUMO level by ca. 0.37 (B3LYP/3-21G) or 0.35 eV (B3LYP/6-31G*) and similarly increases the adiabatic electron affinity (AEA, see Table S3 in the Supporting Information) by 0.46 (B3LYP/3-21G) or 0.44 eV (B3LYP/6-31G*). The substitution at the imide position with alkyl chains (compound **2c**), as compared with fluoroalkyl chains (**2b**), increases back the LUMO level by 0.27 eV and decreases the AEA by 0.28 eV at both levels of theory. Interestingly, the transport gap [ΔE(HOMO − LUMO)] is weakly affected by the substitution and is identical for compounds **2b** and **2c**, while it is slightly smaller for compound **1a** as a result of the increased conjugation associated with the planar perylene chromophore in the latter.

The AP-computed intramolecular reorganization energies (collected in Tables S3 and S4 in the Supporting Information): 0.31, 0.36, and 0.35 eV for compounds **1a**, **2b**, and **2c**, respectively (values smaller by 0.01 eV with the 6-31G* basis set) are relatively large, and a fraction of their magnitude can be attributed to the presence of the bay and imide flexible substituents. To investigate this effect in more detail, we carried out quantum-chemical calculations on model systems for the **1a**, **2b**, and **2c** compounds, featuring the minimal substituents mimicking the steric and electron-withdrawing effect of fluoroalkyl and alkyl substitutents but at the same time reducing the number of flexible degrees of freedom. To this end, we selected the two model systems depicted in Figure 2, featuring a methyl group at the imide position in conjunction with (a) hydrogens in the bay region (**1a**-model) leaving a planar conjugated framework as for **1a** or (b) a CF_3 substituent (**2b**-**2c**-model) in the bay region, which should provide a realistic representation of compounds **2c** or **2b** with regard to their structural characteristics. Indeed, comparison between computed geometry changes upon electron transfer shows minimal differences between model and real systems (see Figures S4 and S5 in the Supporting Information), thereby showing that the chosen models are realistic. Similarly, the frontier orbitals of the model and real systems are very similar (see Figures S6 and S7 in the Supporting Information). Interestingly, the intramolecular reorganization energies computed for the model systems are 0.26 (0.26) and 0.28 (0.30) eV for **1a**-model and **2b**-**2c**-model, respectively, at the B3LYP/3-21G (B3LYP76-31G*) levels of theory. These values, as those computed for the real systems, are in line with previously reported values for PBI derivatives.[40] The difference (0.05−0.08 eV) between the computed λ_i for model and real systems suggests that the presence of flexible substituents (in the real **1a**, **2b**, and **2c** systems) increases the intramolecular parameters, a factor that should be taken into account in the design of new species, because of its role in trapping charge carriers, thereby reducing the charge mobility. The computed vibrational contributions to the intramolecular reorganization energies collected in Figures S8−S11 in the Supporting Information are indeed similar for model (**1a**-model or **2b**-**2c**-model) and correspondingly real (**1a** or **2b** and **2c**) systems except for the fact that in real systems a number of additional contributions are located in the low frequency region; hence, it can be attributed to the increased number of flexible (low frequency) degrees of freedom. Adapting the intramolecular effective parameters computed for model compounds to the respective real systems and including the exceeding contributions from low frequency modes into the λ_{class} parameter (see the Supporting Information and Table S5), we estimated the rate constants of **1a**, **2b**, and **2c** according to eq 1.

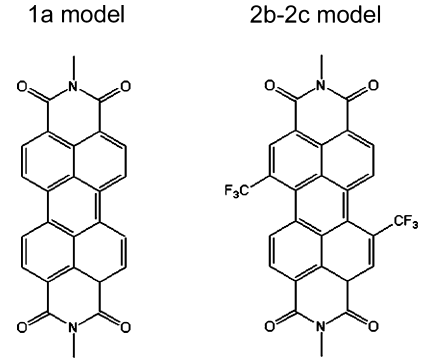

Figure 2. Structural formula of the two model PBI derivatives considered in this work.

3.2. Intermolecular Charge Transport Parameters. The assumption of the hopping mechanism for the charge transport in crystals of PBI derivatives is justified because of the relatively large value of the λ_i parameter. To investigate the possible hopping paths, we extracted, for each crystal, all of the possible neighbors of a given molecule. The crystals of the PBI derivatives investigated in this work belong to the same triclinic $P\bar{1}$ group. However, while there is only one site in the crystal of **1a**, there are two different sites (corresponding to the two enantiomers of the twisted PBI) for **2b** and **2c**. As for other PBI derivatives,[9,14,15] the tendency to form columns of π-stacked PBI units is clearly seen in Figure S2 of the Supporting Information and Figures 3−5. Accordingly, the charge transport can be discussed in terms of *intracolumn* jumps and *intercolumn* jumps as pictorially shown in Figures 3−5. In Table 1, we collected the calculated charge transfer integrals for the various hopping paths in the three crystals. It is worth noting that while there is only one type of intracolumn jump (labeled A) for **1a** (see Figure 3), there are two kinds of intracolumn jumps (labeled A and B) in the crystals of **2b** and **2c**, as graphically depicted with blue and red arrows in Figures 4 and 5. The two jumps for **2b** and **2c** are due to the presence of two different molecular sites, which imply that given one molecular site, the jumps to a different one, in backward and forward directions, are characterized by different charge transfer integrals V_{ij}. Such difference is larger for **2b** than for **2c**.

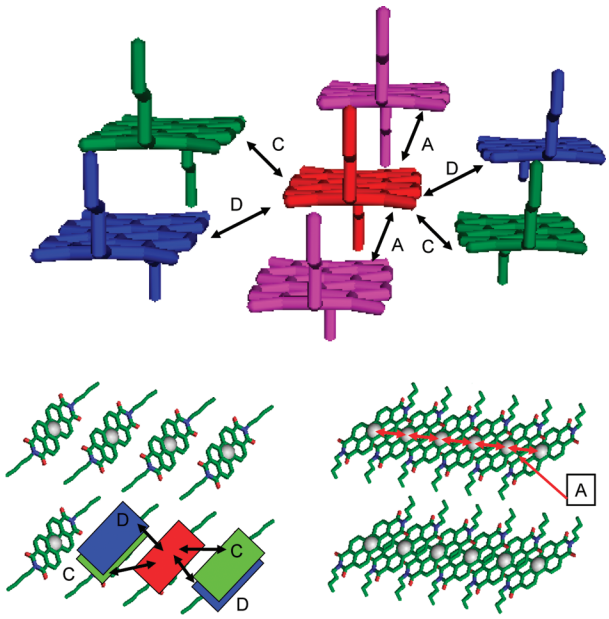

Figure 3. Crystal of **1a**. (Top) The possible intra- (magenta molecules) and intercolumn (green and blue molecules) paths taking as reference the red central molecule. The capital letters indicate the jumps that are active because of non-negligible charge transfer integrals. (Bottom) Schematic indication of (left) the intercolumn paths C and D and (right) the intracolumn path A. The sequence of red arrows underscores that the jumps along the column are identical. The white spheres centered on each molecule represent the centers of mass, and hydrogen and fluorine atoms are omitted.

Inspection of Table 1 shows that the intracolumn jump for compound **1a** is associated with a remarkably small charge transfer integral. However, the optimal packing induced by intermolecular forces in organic crystals corresponds, in some cases, to minimization of the molecular orbital superposition; hence, it is not surprising that the charge transfer integral is minimal at the crystal structure. To quantify the relevance of this effect, we computed (see Figure 6) the charge transfer integral for a dimer of PBI starting from its face to face configuration and by translating one molecule with respect to the other along the long and short molecular axes. The configuration of the dimer in the crystal of **1a** corresponds to a translation of the long axis by ca. 3.4 Å and of the short axis by ca. 1.2 Å and is represented by the black square in Figure 6. The corresponding behavior of the V_{ij} integral as a function of the translation along the short axis is represented by the blue curve in Figure 6. It is seen that the translation is accompanied by a large variation in the charge transfer integral as expected because of the variation in the overlap between the LUMO orbitals of the two molecules (shown in the insets of Figure 6). As a consequence, vibrational motions (and therefore thermally induced disorder) may lead to significant values of the intracolumn charge transfer integral. A complete study of the dynamically induced modulation of charge transfer integrals is beyond the scope of this work and will be the subject of future investigations. However, preliminary molecular dynamics simulations (outlined in the Supporting Information) along the lines described in ref 41 indicate that the modulation of charge transfer integrals at ca. 300 K can be fitted with a Gaussian distribution (see Figure S12 in the Supporting Information) whose σ is of the order of few hundreds cm^{-1}. Thus, we can account for the effect of thermally induced disorder by considering the thermalized limit[42] for this specific jump, that is, by injecting the $\langle V_{ij}^2 \rangle$ value into the MLJ expression for the rate constant, as generally done in the description of biological systems, an approach whose derivation and validity has been recently discussed.[42−45] The thermalized limit is acceptable in this case since the frequency of intermolecular modes is larger than the hopping frequency for the A jump. Because $\langle V_{ij} \rangle$ is almost negligible, $\langle V_{ij}^2 \rangle = \sigma^2$ and jump A are expected to be more dramatically affected by thermal disorder. Thus, we run two set of KMC simulations, using both the static crystal value of V_{ij} and the estimated $\sqrt{\langle V_{ij}^2 \rangle}$ value (assuming an upper limit of 600 cm^{-1} for σ) for the **1a** system (see Table 1).

Inspection of Table 1 and Figures 3−5 shows that, beside the intracolumn charge transfer integrals, also intercolumn jumps are active because of non-negligible electronic couplings. While the intercolumn distance is relatively large for crystals of **2b** and **2c**, because of the presence of alkylated substituents in the bay region, it is much closer in the crystal of **1a**. For instance, the most efficient intercolumn jump in **1a** must overcome 9.19 Å as compared with 11.82 Å for the crystal of **2c** and 13.30 Å for **2b**. The shortest distance in the case of **1a** is associated with a considerable charge transfer coupling of 338 cm^{-1} for path C. In contrast, modest charge transfer integrals are computed for both **2b** and **2c** (see Table 1).

3.3. Charge Transfer Rate Constants and KMC Simulations. With the parameters discussed above, we computed the charge transfer rate constants (collected in Table 1) and injected them into the KMC scheme[14,31−37] to estimate charge transport mobilities at 300 K. The absolute magnitude of charge mobilities can be influenced by the choice of the intra- and intermolecular parameters entering the definition of the charge transport rate constant. Some of these parameters, such as the outer sphere contribution to the reorganization energy, are difficult to estimate[46] and can affect the resulting values. In addition, the model assumes a perfect crystal structure without defects or microcrystalline boundaries while measurements are generally carried out in films whose exact morphology is not known. Thus, the purpose is not to reproduce the experimental values but to provide correct trends for relative values and to rationalize why different mobilities are obtained for different molecular and crystal architectures. In this sense, it is interesting to note (see Table 2) that the order of computed mobilities agrees with that experimentally found. More precisely, the smallest mobility is computed for compound **2b**; as observed, a larger mobility is computed for compound **2c**, and the largest value is computed for **1a**, in agreement with the observation. Notice that the correct order is also obtained without using the thermalized limit for the A jump of system **1a** (compare the computed charge mobilities in the fourth column of Table2) or even assuming an identical value of the λ_{class} parameter (see eq 1) for all of the systems investigated.

We can analyze the computed mobilities in terms of charge transfer integrals, rate constants, and the arrangement of charge transfer paths available to each PBI derivative investigated. With regard to the electronic couplings, compound **2b** shows the largest value for an intracolumn jump. Nevertheless, its mobility is computed to be the lowest. The largest intramolecular reorganization energy of **2b** (see Tables S3 and S4 in the Supporting Information) value may contribute to lower the efficiency of charge transport. However, the computed rate constant associated with jump A in Table 1 is larger than the largest K_{eT} of **2c**. The lower mobility of **2b** as compared to **2c** (and to **1a**) is mostly due to a *retardation effect* induced by the different charge transfer probabilities associated with intracolumn paths A and B along the same intracolumn direction. The alternation of A and B jumps along the column, schematically

TABLE 1: Charge Transfer Integrals V_{ij} (cm^{-1}) and Rate Constant k_{eT} (ps^{-1}) for the Most Relevant Dimers of 1a, 2b, and 2c Extracted from the Crystal Structures

dimer	intracolumn distance (Å)	V_{ij}^{LUMO} (cm^{-1})[a]	k_{eT}[b] (ps^{-1})	dimer	intercolumn distance (Å)	V_{ij}^{LUMO} (cm^{-1})[a]	k_{eT}[b] (ps^{-1})
1a							
A	4.9104	−23	0.012	C	9.1891	338	2.3
		600[c]	7.2	D	12.0472	−33	0.021
2b							
A	6.2112	−772	5.2	C	13.2960	7	0.0005
B	6.3033	282	0.70	D	15.1341	18	0.003
2c							
A	5.8727	−465	2.7	C	10.6947	−10	0.001
B	6.2298	603	4.4	D	11.8171	39	0.018
				E	12.0177	9	0.001

[a] Charge transfer integrals were evaluated at the B3LYP/3-21G level. The interaction was determined between the LUMO orbitals of the two molecules belonging to the dimer. [b] Charge transfer rate constant computed at 300 K. [c] Estimated as an upper limit for $\sqrt{\langle V_{ij}^2 \rangle}$; see the discussion in the text.

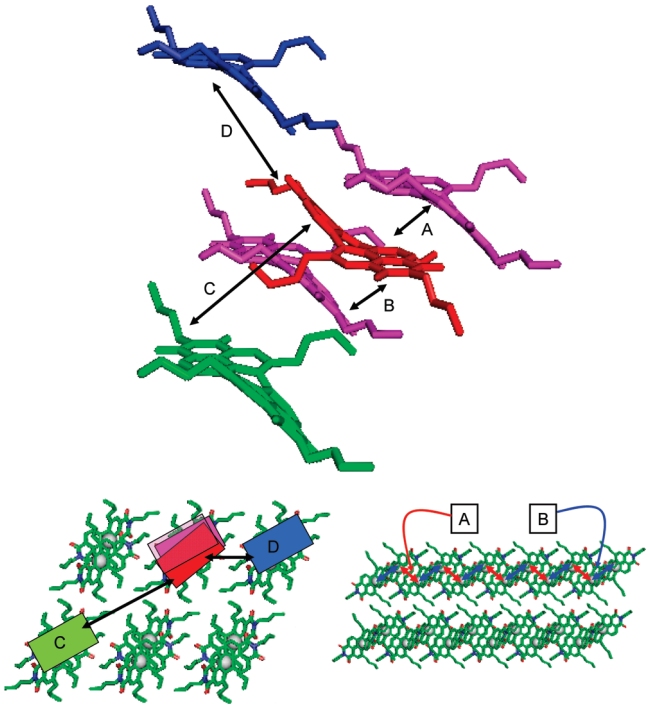

Figure 4. Crystal of **2b**. (Top) The possible intra- (magenta molecules) and intercolumn (green and blue molecules) paths taking as reference the red central molecule. The capital letters indicate the jumps that are active because of non-negligible charge transfer integrals. (Bottom) Schematic indication of (left) the intercolumn paths C and D and (right) the intracolumn paths A (red arrows) and B (blue arrows). The sequence of red and blue arrows underscores that two different jumps (fast and slow) alternate along the column. The absence of the counterpart of jumps C and D in opposite directions, starting from the same red molecule, underscores the asymmetry that also characterizes intercolumnar jumps. The white spheres centered on each molecule represent the centers of mass, and hydrogen and fluorine atoms are omitted. The two different orientations of the rectangles reflect the presence of two different molecular sites in the crystal.

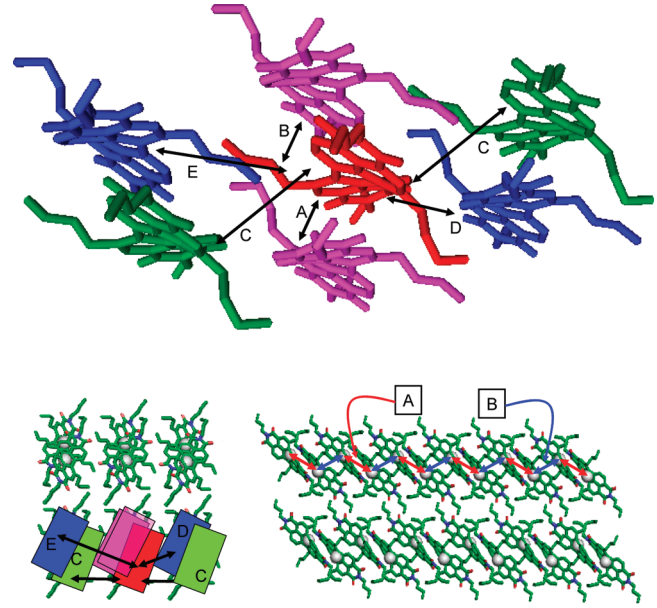

Figure 5. Crystal of **2c**. (Top) The possible intra- (magenta molecules) and intercolumn (green and blue molecules) paths taking as reference the red central molecule. The capital letters indicate the jumps that are active because of non-negligible charge transfer integrals. (Bottom) Schematic indication of (left) the intercolumn paths C, D, and E and (right) the intracolumn paths A (red arrows) and B (blue arrows). The sequence of red and blue arrows underscores that two different jumps alternate along the column. The counterpart of jump D, in opposite direction starting from the same red molecule, is path E. The counterpart of jump C, in opposite direction starting from the same red molecule, is still path C since the molecular sites involved in the jump are of the same type. The white spheres centered on each molecule represent the centers of mass, and hydrogen and fluorine atoms are omitted. The two different orientations of the rectangles reflect the presence of two different molecular sites in the crystal.

shown by red and blue arrows in Figure 4, implies that the charge carrier can propagate along the column by alternating fast and slow jumps. As a result, the charge transport along one PBI column is retarded by the frequent oscillation of the charge trapped in a dimer and it "looses time" before it can find its way one molecule forward along the column. This effect is evident by inspecting a short portion of the KMC trajectory (see Figure 7) showing the propagation of the charge for system **2b**,**c** and **1a** as a function of time. The comparison shows that, for system **2b**, the charge carrier is more frequently trapped (black rectangles in the figure) inside the same dimer, without advancing. The effect is visible also for **2c**, although it is less extensive and frequent because of the lower asymmetry of A−B jump probability (see Table 1). Thus, asymmetry in the backward and forward charge transfer probabilities along a given direction leads to a retardation effect, which is larger for larger asymmetries, namely, for compound **2b** than for compound **2c**. Accordingly, for system **1a**, there is no trace of retardation effect in Figure 7. In passing, we note that such retardation effect is at the origin of a further remarkable discrepancy between the charge mobilities computed using the KMC procedure or

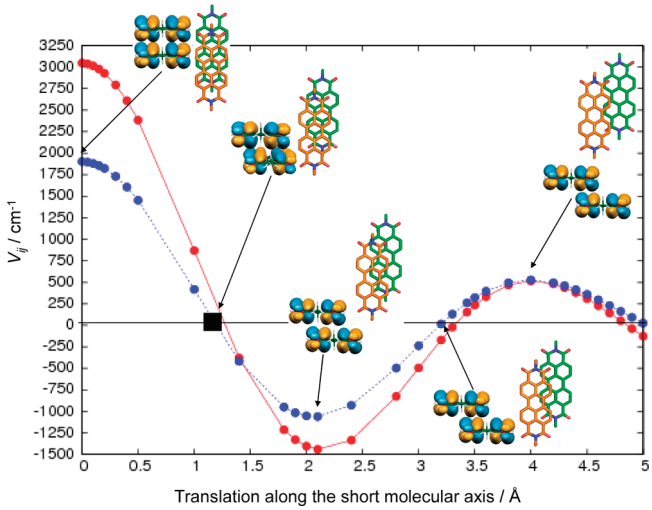

Figure 6. Dependence of the charge transfer integral V_{ij} associated to the A jump, as a function of the sliding along the short axis for selected values of the sliding along the long molecular axis, keeping the intermolecular distance fixed to the value observed in the crystal. The red curve corresponds to translation along the short axis, starting from a face to face dimer. The blue curve corresponds to translation along the short axis starting from the dimer configuration in the crystal, which is represented by the black square in the figure.

employing the approximate formulation of the diffusion coefficient based on isotropic diffusion, often used in previous works.[47,48]

The asymmetry discussed for the intracolumn charge transfer probabilities of **2b** and **2c** and responsible for the retardation effect extends also to intercolum paths if two different molecular sites (the two enantiomeric forms) form the dimer: In this case, the k_{eT} associated with the jump in one direction or in the opposite direction, starting from the same molecule, are not identical (see Table 1). In the case of **2b**, the intercolumn jumps associated with non-negligible charge transfer probabilities are indicated in Figure 4: The asymmetry effect is dramatic, and the jumps labeled C and D do not have a counterpart (negligible charge transfer probabilities) in the opposite direction, starting from the same red molecule in the figure. In addition, the efficiency of intercolumn jumps in **2b** (and also **2c**) is modest (see Table 1) as compared to **1a**. As a result, jumps from the red molecule (in Figure 4) to nearby PBI columns occur only in one direction, and charge carriers for **2b** are expected to propagate mainly along columns of PBI stacked molecules, with seldom jumps from one column to another. This expectation is confirmed by the KMC simulations, as shown by the selected trajectories in Figures S13 and S14 in the Supporting Information.

The pattern of possible intercolumn jumps is slightly more symmetric for **2c**. In this case, as shown in Figure 5, the forward and backward jumps D and E are both associated with non-negligible charge transfer integrals and rate constants. We note, in passing, that the two jumps labeled C in Figure 5 are identical since the dimer involves two identical molecular sites (that is the same enantiomeric form) in the crystal. Nevertheless, even for **2c**, KMC simulations show a dominant charge propagation along the π-stacked PBI columns with less frequent jumps to nearby columns (see Figures S15 and S16 in the Supporting Information).

The large charge transfer integral associated with intercolumn path C of **1a** (Figure 3 and Table 1) implies that these intercolumn jumps are relatively efficient and, together with the

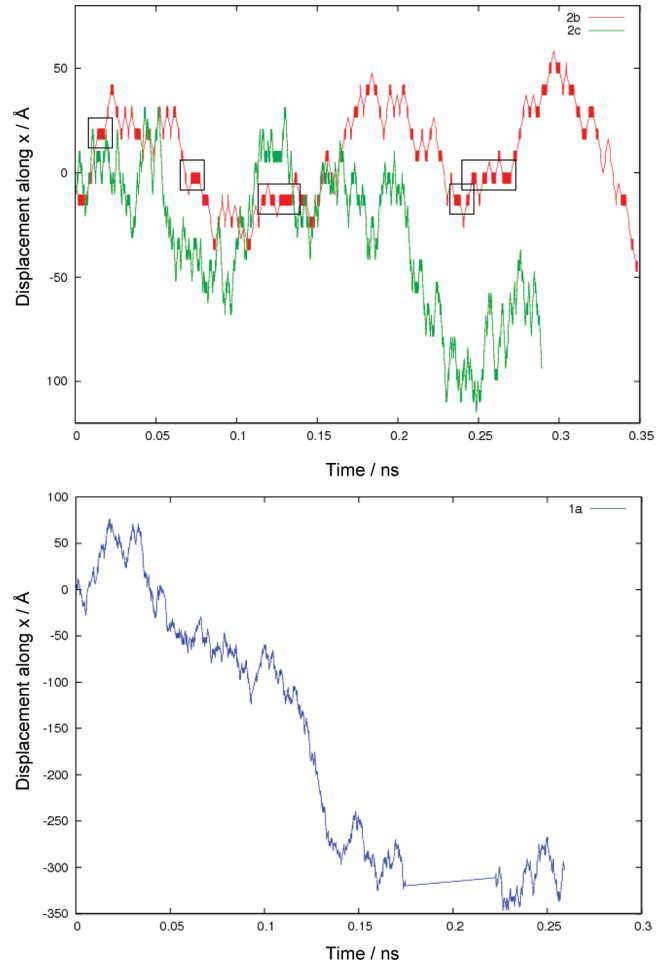

Figure 7. First 1000 steps of a KMC trajectory of a charge carrier propagating along a crystal of (top) **2b** (red) and **2c** (green). The trajectory of **2b** shows frequent oscillations (some of which are enclosed in black rectangles) induced by the presence of markedly alternating fast and slow paths ABABAB along the column. These oscillations do not advance the charge carrier and induce a "retardation effect". The charge is trapped several times and keeps oscillating back and forth in a dimer before it finds its way along the column. The retardation effect is less marked in **2c** because of the similar probability associated with paths A and B. (Bottom) For comparison, the first 1000 steps of a carrier propagating in **1a** (blue), for which a single path A is repeated along the column, show no evidence of a retardation effect.

intracolumn propagation along path A, lead to a quasi bidimensional conduction of the charge as seen in Figure S17 in the Supporting Information, showing the path followed by the charge carrier in a series of KMC trajectories. In contrast, neglecting thermally induced disorder, a quasi monodimensional conduction would result along the intercolumn path C (see Figure S18 in the Supporting Information).

We can conclude that system **1a** shows the largest mobility because of its smaller intramolecular reorganization energies combined with large intercolumn and intracolumn charge transfer integrals and the absence of asymmetries inducing retardation effects. In contrast, systems **2b** and **2c** show similarly large charge transfer integrals whose effect is depressed by the presence of larger intramolecular reorganization energies (leading to reduced rate constants) combined with the retardation effect induced by the asymmetry of alternating fast and slow paths along the intracolumn direction. Although the order of computed charge mobilities is correct, the mobility of **2c** is computed to be ca. 2 times larger than that of **2b** while experimentally[18] a ratio of 17 is found. This suggests that other

TABLE 2: Computed Electron Mobilities μ ($cm^2\ V^{-1}\ s^{-1} \times 10^2$) for the Crystals of PBI Derivatives 1a, 2b, and 2c[a]

	only intracolumn paths 10^6 MC steps	intracolumn (thermalized limit) and intercolumn paths 10^8 MC steps	intracolumn and intercolumn paths 10^8 MC steps (10^7 MC steps)
1a		8.00	4.21 (4.25)
2b	2.21		1.12 (1.12)
2c	5.88		1.91 (1.92)

[a] Data averaged over 15 groups of 2000 trajectories.

factors are likely to influence the experimental values, such as, for instance, the presence of defects or traps.

4. Concluding Remarks

We have investigated the charge transport properties of three PBI derivatives with enhanced n-type character. Quantum-chemical calculations show that fluorination enhances the n-type character by lowering the LUMO levels and increasing the computed electronic affinities.

The solid state structure of the three systems investigated is characterized by the presence of π-stacked PBI columns in which the PBI sites are identical for compound **1a**, while the two enantiomeric forms of the twisted PBIs **2b** and **2c** alternate as two different molecular sites along the column. This characteristic implies an asymmetry in the charge transfer probability along a given direction, particularly relevant along the intracolumn propagation direction.

Calculations of charge transfer rate constants, according to the nonadiabatic hopping approach, and propagation of the charge carriers within a KMC scheme lead to predicted charge mobilities whose relative order is in agreement with the experimental results. The mobility of **2c** is correctly predicted to be larger than that of **2b**, and the charge mobility of **1a** is computed to be the largest. The larger observed ratio between the mobilities of **2c** and **2b** is attributed to the presence of defects and traps.

For compound **1a**, the crystal packing of PBI units minimizes the intracolumn charge transfer integrals. Even in the absence of thermally induced disorder effects, the KMC simulations predict the largest mobility for **1a**. Preliminary calculations including the thermalized limit of the charge transfer integral increase considerably the intracolumn component of the charge mobility. Because of the smaller intercolumn distance in **1a**, a considerable contribution to the total charge mobility arises from intercolumn charge transport and leads to a quasi bidimensional character of the charge transport.

The simulations indicate, instead, preferential intracolumn conduction for **2b** and **2c**. A careful analysis of intramolecular and intermolecular factors reveals that a major effect determining the lower mobility of **2b** and **2c** as compared to **1a** and, between the former two, a lower mobility for **2b**, is a pronounced *retardation effect* in turn governed by the asymmetry in the charge transfer probability along a given direction. Indeed, the charge propagation for the two systems occurs mostly along the π-stacked PBI columns and the probability associated with the two alternating paths A and B is more markedly different for **2b** than for **2c**.

Overall, the study reveals that asymmetry in charge transfer probabilities along a given direction may reduce drastically the charge mobility and that the mono- or bidimensional character of the charge propagation can be governed by appropriate use of substituents. In more general terms, the study discloses the subtle interplay between intramolecular and intermolecular contributions to the efficient charge carrier propagation in an organic semiconductor to guide the design of more efficient organic semiconductors.

Acknowledgment. We acknowledge grants from MIUR: ex 60% and PRIN Project 2008 JKBBK4 "Tracking ultrafast photoinduced intra- and inter-molecular processes in natural and artificial photosensors". We are indebted to Prof. Giorgio Orlandi for useful discussions.

Supporting Information Available: Details on computational models, five tables including absolute energies for all of the computed structures, frontier molecular orbital energies, intermolecular reorganization energies, computed electron affinities, and parameters employed to estimate charge transfer rate constants. Eighteen figures including a schematic representation of electron affinities and reorganization energies, the crystal structure of the systems investigated, the geometry change upon charging for the PBI derivatives investigated, the frontier molecular orbitals, the vibrational contribution to intramolecular reorganization energies, the dispersion of charge transfer integrals, and a selection of computed KMC trajectories. This material is available free of charge via the Internet at http://pubs.acs.org.

References and Notes

(1) Horowitz, G.; Kouki, F.; Spearman, P.; Fichou, D.; Nogues, C.; Pan, X.; Garnier, F. *Adv. Mater.* **1996**, *8*, 242–245.
(2) Schmidt-Mende, L.; Fechtenkoetter, A.; Muellen, K.; Moons, E.; Friend, R. H.; MacKenzie, J. D. *Science* **2001**, *293*, 1119–1122.
(3) Zang, L.; Che, Y. K.; Moore, J. S. *Acc. Chem. Res.* **2008**, *41*, 1596–1608.
(4) Qian, H. L.; Negri, F.; Wang, C. R.; Wang, Z. H. *J. Am. Chem. Soc.* **2008**, *130*, 17970–17976.
(5) Qian, H. L.; Yue, W.; Zhen, Y. G.; Di Motta, S.; Di Donato, E.; Negri, F.; Qu, J. Q.; Xu, W.; Zhu, D. B.; Wang, Z. H. *J. Org. Chem.* **2009**, *74*, 6275–6282.
(6) Zhen, Y. G.; Qian, H. L.; Xiang, J. F.; Qu, J. Q.; Wang, Z. H. *Org. Lett.* **2009**, *11*, 3084–3087.
(7) Qian, H. L.; Wang, Z. H.; Yue, W.; Zhu, D. B. *J. Am. Chem. Soc.* **2007**, *129*, 10664–10665.
(8) Schmidt, R.; Ling, M. M.; Oh, J. H.; Winkler, M.; Konemann, M.; Bao, Z. N.; Wurthner, F. *Adv. Mater.* **2007**, *19*, 3692–3695.
(9) Schmidt, R.; Oh, J. H.; Sun, Y. S.; Deppisch, M.; Krause, A. M.; Radacki, K.; Braunschweig, H.; Konemann, M.; Erk, P.; Bao, Z. A.; Wurthner, F. *J. Am. Chem. Soc.* **2009**, *131*, 6215–6228.
(10) Oh, J. H.; Liu, S.; Bao, Z.; Schmidt, R.; Wurthner, F. *Appl. Phys. Lett.* **2007**, *91*, 212107.
(11) Ling, M. M.; Erk, P.; Gomez, M.; Koenemann, M.; Locklin, J.; Bao, Z. N. *Adv. Mater.* **2007**, *19*, 1123–1127.
(12) Gsanger, M.; Oh, J. H.; Konemann, M.; Hoffken, W.; Krause, A. M.; Bao, Z.; Wurthner, F. *Angew. Chem., Int. Ed. Engl.* **2010**, *49*, 740–743.
(13) Brooks, A. J.; Facchetti, A.; Wasielewski, M. R.; Marks, T. J. *J. Am. Chem. Soc.* **2007**, *129*, 15259–15278.
(14) Marcon, V.; Breiby, D. W.; Pisula, W.; Dahl, J.; Kirkpatrick, J.; Patwardhan, S.; Grozema, F.; Andrienko, D. *J. Am. Chem. Soc.* **2009**, *131*, 11426–11432.
(15) Hansen, M. R.; Graf, R.; Sekharan, S.; Sebastiani, D. *J. Am. Chem. Soc.* **2009**, *131*, 5251–5256.
(16) Chen, Z. J.; Baumeister, U.; Tschierske, C.; Wurthner, F. *Chem.—Eur. J.* **2007**, *13*, 450–465.
(17) Ruiz Delgado, M. C.; Pigg, K. R.; Da Silva Filho, D. A.; Gruhn, N. E.; Sakamoto, Y.; Suzuki, T.; Osuna, R. M.; Casado, J.; Hernandez, V.;

Navarrete, J. T. L.; Martinelli, N. G.; Cornil, J.; Sanchez-Carrera, R. S.; Coropceanu, V.; Bredas, J. L. *J. Am. Chem. Soc.* **2009**, *131*, 1502–1512.

(18) Li, Y.; Tan, L.; Wang, Z. H.; Qian, H. L.; Shi, Y. B.; Hu, W. P. *Org. Lett.* **2008**, *10*, 529–532.

(19) Bredas, J. L.; Beljonne, D.; Coropceanu, V.; Cornil, J. *Chem. Rev.* **2004**, *104*, 4971–5003.

(20) Coropceanu, V.; Cornil, J.; da Silva, D. A.; Olivier, Y.; Silbey, R.; Bredas, J. L. *Chem. Rev.* **2007**, *107*, 926–952.

(21) Coropceanu, V.; Andre, J. M.; Malagoli, M.; Bredas, J. L. *Theor. Chem. Acc.* **2003**, *110*, 59–69.

(22) Orlandi, G.; Troisi, A.; Zerbetto, F. *J. Am. Chem. Soc.* **1999**, *121*, 5392–5395.

(23) Troisi, A.; Orlandi, G. *Chem. Phys. Lett.* **2001**, *344*, 509–518.

(24) Fujita, T.; Nakai, H.; Nakatsuji, H. *J. Chem. Phys.* **1996**, *104*, 2410–2417.

(25) Farazdel, A.; Dupuis, M.; Clementi, E.; Aviram, A. *J. Am. Chem. Soc.* **1990**, *112*, 4206–4214.

(26) Frisch, M. J.; Trucks, G. W.; Schlegel, H. B.; Scuseria, G. E.; Robb, M. A.; Cheeseman, J. R.; Montgomery, J. A., Jr.; Vreven, T.; Kudin, K. N.; Burant, J. C.; Millam, J. M.; Iyengar, S. S.; Tomasi, J.; Barone, V.; Mennucci, B.; Cossi, M.; Scalmani, G.; Rega, N.; Petersson, G. A.; Nakatsuji, H.; Hada, M.; Ehara, M.; Toyota, K.; Fukuda, R.; Hasegawa, J.; Ishida, M.; Nakajima, T.; Honda, Y.; Kitao, O.; Nakai, H.; Klene, M.; Li, X.; Knox, J. E.; Hratchian, H. P.; Cross, J. B.; Bakken, V.; Adamo, C.; Jaramillo, J.; Gomperts, R.; Stratmann, R. E.; Yazyev, O.; Austin, A. J.; Cammi, R.; Pomelli, C.; Ochterski, J. W.; Ayala, P. Y.; Morokuma, K.; Voth, G. A.; Salvador, P.; Dannenberg, J. J.; Zakrzewski, V. G.; Dapprich, S.; Daniels, A. D.; Strain, M. C.; Farkas, O.; Malick, D. K.; Rabuck, A. D.; Raghavachari, K.; Foresman, J. B.; Ortiz, J. V.; Cui, Q.; Baboul, A. G.; Clifford, S.; Cioslowski, J.; Stefanov, B. B.; Liu, G.; Liashenko, A.; Piskorz, P.; Komaromi, I.; Martin, R. L.; Fox, D. J.; Keith, T.; Al-Laham, M. A.; Peng, C. Y.; Nanayakkara, A.; Challacombe, M.; Gill, P. M. W.; Johnson, B.; Chen, W.; Wong, M. W.; Gonzalez, C.; Pople, J. A. *Gaussian 03*, revision C.02; Gaussian, Inc.: Wallingford, CT, 2003.

(27) Cheung, D. L.; Troisi, A. *Phys. Chem. Chem. Phys.* **2008**, *10*, 5941–5952.

(28) Marcus, R. A. *J. Chem. Phys.* **1956**, *24*, 966–978.

(29) Jortner, J. *J. Chem. Phys.* **1976**, *64*, 4860–4867.

(30) Song, Y.; Di, C.; Yang, X.; Li, S.; Xu, W.; Liu, W.; Yang, L.; Shuai, Z.; Zhang, D.; Zhu, D. *J. Am. Chem. Soc.* **2006**, *128*, 15940–15941.

(31) Tan, L.; Zhang, L.; Jiang, X.; Yang, X. D.; Wang, L. J.; Wang, Z.; Li, L. Q.; Hu, W. P.; Shuai, Z. G.; Li, L.; Zhu, D. B. *Adv. Funct. Mater.* **2009**, *19*, 272–276.

(32) Nan, G. J.; Yang, X. D.; Wang, L. J.; Shuai, Z. G.; Zhao, Y. *Phys. Rev. B* **2009**, *79*, 115203.

(33) Yang, X. D.; Wang, L. J.; Wang, C. L.; Long, W.; Shuai, Z. G. *Chem. Mater.* **2008**, *20*, 3205–3211.

(34) Martinelli, N. G.; Savini, M.; Muccioli, L.; Olivier, Y.; Castet, F.; Zannoni, C.; Beljonne, D.; Cornil, J. *Adv. Funct. Mater.* **2009**, *19*, 3254–3261.

(35) Athanasopoulos, S.; Kirkpatrick, J.; Martinez, D.; Frost, J. M.; Foden, C. M.; Walker, A. B.; Nelson, J. *Nano Lett.* **2007**, *7*, 1785–1788.

(36) Olivier, Y.; Lemaur, V.; Bredas, J. L.; Cornil, J. *J. Phys. Chem. A* **2006**, *110*, 6356–6364.

(37) Andrienko, D.; Kirkpatrick, J.; Marcon, V.; Nelson, J.; Kremer, K. *Phys. Status Solidi B* **2008**, *245*, 830–834.

(38) Fichthorn, K. A.; Weinberg, W. H. *J. Chem. Phys.* **1991**, *95*, 1090–1096.

(39) Wurthner, F. *Pure Appl. Chem.* **2006**, *78*, 2341–2349.

(40) Li, C.; Mishchenko, A.; Li, Z.; Pobelov, I.; Wandlowski, T.; Li, X. Q.; Wurthner, F.; Bagrets, A.; Evers, F. *J. Phys.: Condens. Matter* **2008**, *20*, 374122.

(41) Di Motta, S.; Di Donato, E.; Negri, F.; Orlandi, G.; Fazzi, D.; Castiglioni, C. *J. Am. Chem. Soc.* **2009**, *131*, 6591–6598.

(42) Martinelli, N. G.; Olivier, Y.; Athanasopoulos, S.; Delgado, M. C. R.; Pigg, K. R.; da Silva, D. A.; Sanchez-Carrera, R. S.; Venuti, E.; Della Valle, R. G.; Bredas, J. L.; Beljonne, D.; Cornil, J. *ChemPhysChem* **2009**, *10*, 2265–2273.

(43) Troisi, A.; Nitzan, A.; Ratner, M. A. *J. Chem. Phys.* **2003**, *119*, 5782–5788.

(44) Skourtis, S. S.; Balabin, I. A.; Kawatsu, T.; Beratan, D. N. *Proc. Natl. Acad. Sci. U.S.A.* **2005**, *102*, 3552–3557.

(45) Troisi, A.; Ratner, M. A.; Zimmt, M. B. *J. Am. Chem. Soc.* **2004**, *126*, 2215–2224.

(46) Norton, J. E.; Bredas, J. L. *J. Am. Chem. Soc.* **2008**, *130*, 12377–12384.

(47) Deng, W. Q.; Goddard, W. A. *J. Phys. Chem. B* **2004**, *108*, 8614–8621.

(48) Song, Y. B.; Di, C.; Yang, X. D.; Li, S. P.; Xu, W.; Liu, Y. Q.; Yang, L. M.; Shuai, Z. G.; Zhang, D. Q.; Zhu, D. B. *J. Am. Chem. Soc.* **2006**, *128*, 15940–15941.

JP101040R